

Load-Displacement Formulations of Low-rise Unbounded RC Shear Walls with or without Openings

K. Y. Lou¹, F. Y. Cheng[†], M. S. Sheu², and X. Z. Zhang³

¹Structural Engineer, Ph.D., Taylor & Gaines Structural Engineers, 320 North Halstead Street Suite 200, Pasadena, CA 91107-3151, USA

[†]Curators' Professor Emeritus, Dept. of Civ. Engrg., Univ. of Missouri-Rolla, Rolla, MO 65409,

²Professor, Architecture Dept., National Cheng-Kung Univ., Tainan, Taiwan

³Ph.D. Candidate, Dept. of Civ. Engrg., Univ. of Missouri-Rolla, Rolla, MO 65409

Received September 2001; Accepted November 2001

ABSTRACT

Investigations of low-rise unbounded reinforced concrete shear walls with or without openings are performed with comparison of analytical and experimental results. Theoretical analysis is based on nonlinear finite element algorithm, which incorporates Ottosen's concrete failure criterion and nonlinear constitutive relationships. Studies focus on the effects of height-to-length ratio of shear walls, opening ratio, horizontal and vertical reinforcement ratios, and diagonal reinforcement. Analytical solutions conform well with experimental results. Equations for cracking, yielding and ultimate loads with corresponding lateral displacements are derived by regression using analytical results and experimental data. Also, failure modes of low-rise unbounded shear walls are theoretically investigated. An explanation of change in failure mode is ascertained by comparing analytical results and ACI code equations. Shear-flexural failure can be obtained with additional flexural reinforcement to increase a wall's capacity. This concept leads to a design method of reducing flexural reinforcement in low-rise bounded solid shear wall's. Avoidance of shear failure as well as less reinforcement congestion for these walls is expected.

Keywords: ACI building code, low-rise shear wall, inelastic, nonlinear finite element, shear-wall boundary element, crack, design, diagonal reinforcement, load-displacement relationship, opening ratio, reinforced concrete, ultimate, yielding.

1. Introduction

Low-rise reinforced concrete (RC) shear walls (i.e., height-to-length ratio not greater than 1.0) can be classified as bounded or unbounded. The former features concentrated vertical reinforcement near ends of the shear wall supported with transverse reinforcement; the latter is characterized by uniform distribution of both vertical and horizontal shear reinforcement.

Low-rise bounded RC shear walls are widely used to provide lateral stiffness for building structures. Considerable interest has focused on their performance since the 1950s. The studies include shear-wall strength under monotonically static loadings (Galletly, 1952; Benjamin and

Williams, 1957; Wood, 1990), dynamic strength (Antebi *et al.*, 1960; Anderson *et al.*, 1964), development of design code provisions (Cardenas *et al.*, 1973), experiments on RC perforated shear walls (Yamada *et al.*, 1974), monotonic or cyclic behavior with flanged boundary elements (Barda *et al.*, 1976, 1977), and load-deflection relationships of low-rise column-bounded RC shear walls (Watabe *et al.*, 1989). The outcome of the research work has led to the development of building code provisions for shear-wall design, such as ACI 318-95 (ACI 1995).

Low-rise unbounded RC shear walls are used in box-type buildings, nuclear power plants, and industrial structures. Cardenas *et al.*, (1980) tested seven low-rise unbounded shear walls to determine their shear strength. Murakami *et al.*, (1989) experimentally demonstrated that unbounded shear walls display adequate shear strength and deformation capacity if boundary elements are eliminated.

From the viewpoint of structural analysis, unbounded

[†] Corresponding author

Tel: +573-341-4469; Fax: +573-341-4729

E-mail address: chengfy@umr.edu

shear walls are modeled as shear-wall elements due to their uniform distribution of reinforcement; bounded shear walls are modeled as column element and shear-wall element. To establish shear-wall elements, however, scant test results are available for shear-wall stiffness under monotonic or cyclic loading. Since structural analysis cannot be performed without proper modeling of shear walls, further experimental and analytical work should be carried out. Cheng and Sheu (2001, 1995, 1994, 1993, 1992, 1991 and 1989) have conducted extensive analytical and experimental work on low-rise unbounded RC shear walls with or without openings. They developed a macro-element model which satisfactorily depicts shear-wall failure mechanism and its hysteresis rules under earthquake-type loading. This model separates shear and bending deformation which allows shear and bending stiffness of a shear-wall element to be established. The model is governed by backbone curve as a force-displacement envelope under cyclic excitation. Backbone curves need to be established for individual wall through mechanics principle and numerical analysis, and then seismic response of a system can be studied.

To simplify the determination of backbone curves for low-rise unbounded shear walls with or without openings, an algorithm of nonlinear finite element analysis (Lou and Cheng 1994) is developed for reinforced concrete members or structures. Computer solutions and test results by Vecchio and Chan (1990) and Sheu (1988) are first compared to demonstrate the reliability of the algorithm. Then the study of low-rise shear walls focuses on the effects of wall height-to-length ratio, opening ratio, horizontal and vertical reinforcement ratio, and diagonal reinforcement; these parameters are essential in the development of backbone curves. After analytical and test results, mathematical equations for cracking, yielding, and ultimate loads with correspondingly lateral displacements are formulated through regression. These critical points form the backbone curve, which can be applied to nonlinear analysis of seismic-resistant structures with shear walls macro-elements. In addition, these proposed equations are useful in engineering practice to predict load and displacement of a wall at any loading stage from elastic through ultimate. Theoretical analysis also investigates the failure modes of shear walls. Comparison between ACI 318-95 building code provisions and analytical results leads to a recommendation for designing flexural reinforcement to obtain shear-flexural failure modes.

2. Nonlinear Finite Element Analysis

2.1 Implementation of Nonlinear Elements

Nonlinear finite element method (NFEM) has been

widely accepted as a powerful tool to analyze RC structures. It can successfully simulate test procedures and satisfactorily predict locations of cracks, crack propagation, reinforcement yielding, ultimate capacity, structural deformations, and the like.

Satisfactory solutions of NFEM mainly depend on the selection of concrete failure criterion and constitutive relationships. Test observations indicate that the failure surface of concrete under triaxial stress conditions exhibits the following characteristics: (1) it is smooth and convex; (2) its meridians in the principal stress coordinate system are parabolic and do not intersect the negative hydrostatic axis; and (3) its tracings in the deviatoric plane vary from nearly triangular to a circular shape with increase of hydrostatic pressure (Chen, 1982).

Concrete failure criterion proposed by Ottosen (1977) satisfies the aforementioned requirements and is therefore adopted in this study. Constitutive model by Ottosen (1979) to determine secant modulus of concrete is also employed herein. An elasto-plastic model is used for reinforcement. Failure criteria and constitutive relationships for both reinforcement and concrete are incorporated into a nonlinear finite element model (Cheng and Lou, 1995). Nonlinear material behavior is accommodated by using secant stiffness method. Concrete is considered as isoparametric hexahedral elements with eight nodes; reinforcement is assumed to be uniformly distributed over concrete elements with a perfect bond between them before concrete cracks. If concrete cracks, a smeared cracking model is applied to deal with the subsequent behavior of concrete. Computer program NARCS for nonlinear finite element analysis is developed for UNIX system (Lou and Cheng, 1994). NARCS is further applied to study RC bridge collapse under seismic excitation (Lou *et al.*, 2001).

2.2 Verification of NFEM results

To verify the reliability of the computer algorithm used herein to predict behavior of low-rise unbounded RC solid and perforated shear walls, comparisons are first performed with test results by Vecchio and Chan (1990) and Sheu (1988).

Vecchio and Chan (1990) tested nine shear panels, divided into three groups. Each group has a solid panel, a panel with a 150-mm square perforation in the center, and a panel with the same opening additionally reinforced around the sides. Load conditions are considered as pure shear (group I), combined shear and biaxial compression (group II), and combined shear and biaxial tension (group III). Dimensions of each panel are 890 mm×890 mm×70




mm. Two layers of reinforcement are evenly oriented parallel to the sides of the panel. Horizontal and vertical reinforcement ratios are 1.65% and 0.82%, respectively.

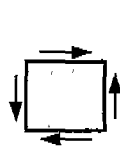
In this analytical work, 288 finite elements are employed for the solid panel, and 280 finite elements for perforated. Loading is incrementally applied until the panel reaches its ultimate capacity. All shear-panel behavior under different loading conditions is reflected in analytical solutions, such as load-displacement relationships at various loading stages of cracking, yielding, and ultimate, and relationships between shear stresses and strains. Cracking, yielding, and ultimate stresses are summarized in Table 1 to compare NFEM and test results. Shear strains from NFEM at cracking, yielding and ultimate stages are also included. But corresponding shear strains from tests are not listed in the table since they are not numerically presented by Vecchio and Chan (1990). Comparisons indicate that analytical and experimental results are similar. It can be seen

that NFEM as employed herein is capable of simulating panel- test results. A good approximation of loading-deformation curves for all the shear panels and a detailed description of analytical results are reported elsewhere by Cheng and Lou (1995).

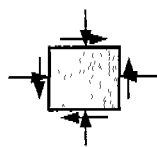
Four low-rise unbounded shear walls tested by Sheu (1988) are selected for comparative studies of load-displacement relationships. These walls are identified as SW-0E, SW-7E, SW-9E, and SW-15E (see Fig. 1). All specimens have a rectangular cross-section 100-mm wide and 1000-mm long. Their height varies between 500 mm and 750 mm, causing changes of height-to-length ratio from 0.50 to 0.75. Dimensions of the center perforation are 654 mm×125 mm for walls 500-mm high, and 654 mm×250 mm for walls 750-mm high. These openings approximate the size of windows which are usually part of shear-wall design. Horizontal and vertical reinforcement ranging from D10 (#3) to D13 (#4) is uniformly dis-

Table 1. Comparison of NFEM and Test Results of Vecchio and Chan (1990)

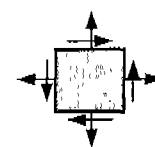
Dimensions of Specimens (mm)	Specimen	Loading Conditions	Cracking Stress σ (MPa) & Strain τ (10^{-3})			Yielding Stress σ (MPa) & Strain τ (10^{-3})			Ultimate Stress σ (MPa) & Strain τ (10^{-3})		
			Test*		NFEM	Test*		NFEM	Test*		NFEM
			σ	τ	σ	τ	σ	τ	σ	τ	σ
 890×890	PC1A	Pure Shear	2.17	0.21	2.05	0.21	5.29	4.89	5.61	5.73	6.72
	PC4	Shear and Compression	3.00	0.39	2.77	0.39	4.75	2.46	4.84	5.01	3.91
	PC7	Shear and Tension	1.50	0.18	1.63	0.18	3.34	4.03	3.65	4.11	6.18
 890×890 150×150	PC2	Pure Shear	1.74	0.32	1.38	0.32	4.10	4.92	4.37	4.33	7.29
	PC5	Shear and Compression	2.32	0.48	1.87	0.48	3.84	2.51	3.84	4.21	4.32
	PC8	Shear and Tension	1.10	0.29	1.16	0.29	2.41	3.81	2.79	2.85	4.76
 890×890 150×150 Added Steel	PC3	Pure Shear	1.90	0.26	1.68	0.26	4.83	5.29	4.83	4.94	6.08
	PC6	Shear and Compression	2.50	0.44	2.17	0.44	3.97	2.64	4.35	4.60	3.95
	PC9	Shear and Tension	1.35	0.23	1.03	0.23	2.86	3.89	3.09	3.35	5.22



Pure Shear



Shear and Compression



Shear and Tension

*Shear strains are not numerically listed by Vecchio and Chan

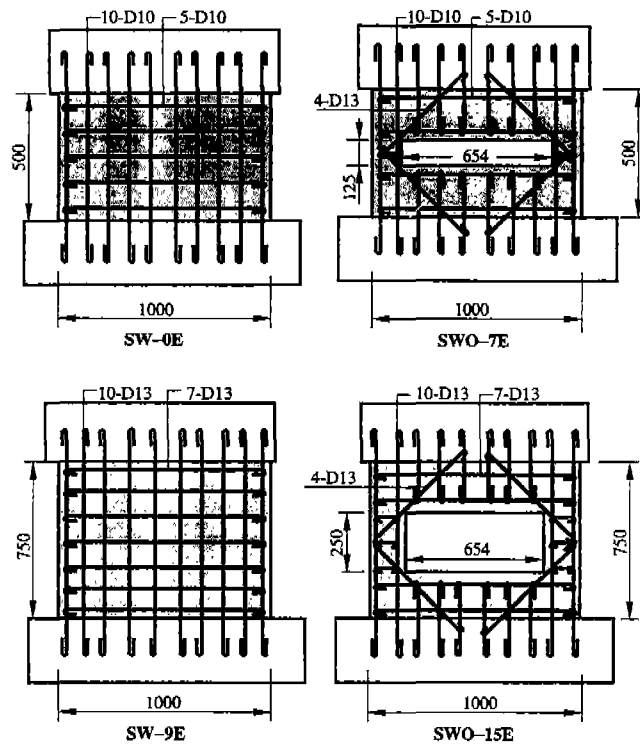


Fig. 1. Specimen Details of Sheu (1988).

Table 2. Material Properties of Selected Shear Walls

Wall	Height h_w (mm)	f'_c MPa	Vertical		Horizontal		Diagonal Bars	f_y MPa	h_w/t_w
			Bars	ρ_v (%)	Bars	ρ_h (%)			
SW-0E	500	25.4	10D10	0.7133	5D10	0.7133	None	510	0.5
SWO-7E	500	32.8	10D10	0.7133	5D10	0.7133	D13	510	0.5
SW-9E	750	29.4	10D13	1.267	7D13	1.183	None	461.7	0.75
SWO-15E	750	27.9	10D13	1.267	7D13	1.183	D13	461.7	0.75

tributed over specimens. D13 (#4) is chosen as diagonal reinforcement. Material properties of these walls are summarized in Table 2.

Specimens SW-0E, SWO-7E, SW-9E, and SWO-15E are divided into 100, 104, 160 and 192 finite elements, respectively. Displacement is prevented at the bottom of the shear wall to simulate experimental conditions. Incrementally lateral forces are evenly distributed at each node on top of the specimen.

To depict the theoretical behavior of shear walls during the entire loading procedure, specimen SW-9E is selected for a detailed description of NFEM results. As shown in Fig. 2(c), the displacement increment of wall SW-9E is proportional to the loading increment at the beginning of loading. During this pre-cracking stage, both finite element analysis and test results present linear behavior. When lateral loading increases to 52.0 kN, cracks occur at

the shear wall's bottom where both concrete and reinforcement elements are in tension. As recorded, experimental crack loading is 45.5 kN, approximately 90 percent of the analytical result. As lateral load increases, more cracks appear and propagate. Due to the uniform distribution of vertical reinforcement and the length of wall, reduction of wall stiffness is prevented at the beginning of cracking. But as loading increases, shear-wall stiffness decreases and the load-displacement relationship deviates from the straight line of pre-cracking stiffness. A sudden increase in calculated displacement after the load of 168 kN is observed due to a reduction of wall stiffness. Vertical reinforcement begins to yield around 290.0 kN, not far from test data (283.7 kN). After vertical reinforcement yields, a small increment of lateral load can lead to a large increment of displacement. Ultimate loading for finite element analysis reaches 336.0 kN, which is close to test data

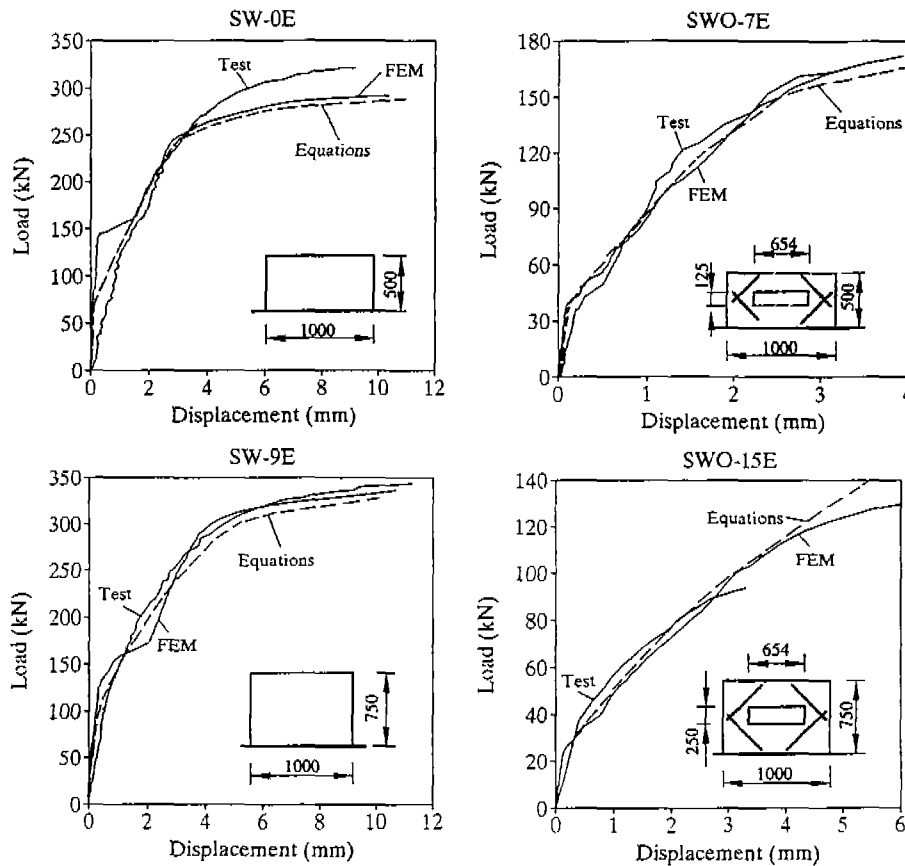


Fig. 2. Comparison of Test and Computer Results and Proposed Equations: (a) SW-0E; (b) SWO-7E; (c) SW-9E; (d) SWO-15E.

(343.1 kN). Theoretical crack patterns at crack and ultimate loading are similar to those recorded experimentally (Cheng and Lou, 1995). Comparison of load-displacement relationships of other specimens, SW-0E, SWO-7E, and SWO-15E, is also shown in Fig. 2 which proves a good conformation between analytical and test results. Again, the reliability of the NFEM algorithm is demonstrated by this comparison.

Note that shear walls with large openings have lower capacity and larger ductility. However, this conclusion is based on walls with the same material properties, such as concrete and reinforcement strength, and reinforcement ratio. If diagonal reinforcement is added in perforated shear walls, its effects on wall ductility may be considered. Fig. 2 illustrates such a situation. For specimen SW-0E, ultimate displacement is about 9.16 mm, while it is 3.14 mm for specimen SWO-7E. Since diagonal reinforcement is placed around the opening of specimen SWO-7E, wall stiffness greatly increases at the post-cracking stage. As loading increases, the perforated shear wall fails with little displacement. That is why specimen SWO-7E reaches its capacity with relatively little displacement. The same phenomenon is also revealed by specimens SW-9E and SWO-15E.

3. Theoretical Studies of Shear Wall Behavior

The behavior of low-rise unbounded shear walls with or without openings is further investigated by applying NFEM. Analytical solutions cover the effects of opening ratio, height-to-length ratio of shear walls, horizontal and vertical reinforcement ratio, and diagonal reinforcement.

To demonstrate that the load-displacement curve of shear walls with openings will converge with that of solid walls, three shear walls with different openings are considered. Wall dimensions are 1000-mm long, 500-mm high, and 100-mm thick. A wall with zero opening ratio is identical to specimen SW-0E. The other two walls have a center perforation of 100×100 mm and 100×200 mm, with ratios of 0.02 and 0.04, respectively. Both horizontal and vertical reinforcement ratios are 0.7133%. Other material properties are the same as specimen SW-0E (see Table 2). A comparison of these three cases is shown in Fig. 3, from which similar shapes of load-displacement curves are observed. If the size of the opening is reduced, then ultimate loading increases and ductility decreases. Note that the load-displacement curve of perforated walls will converge with that of solid walls. Thus a solid shear wall is

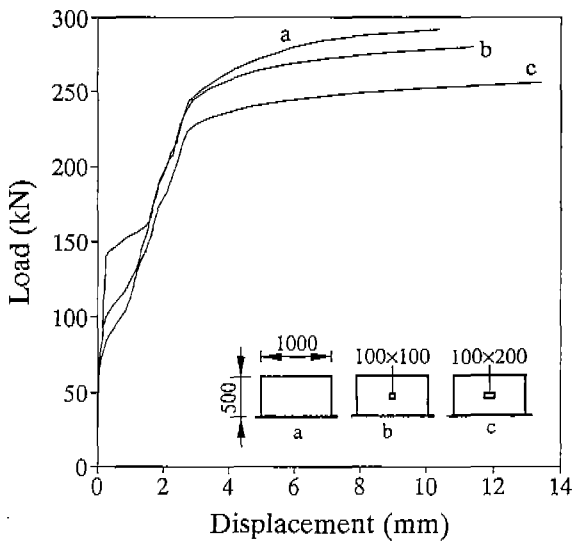


Fig. 3. Load-Displacement Curves with Change of Opening.

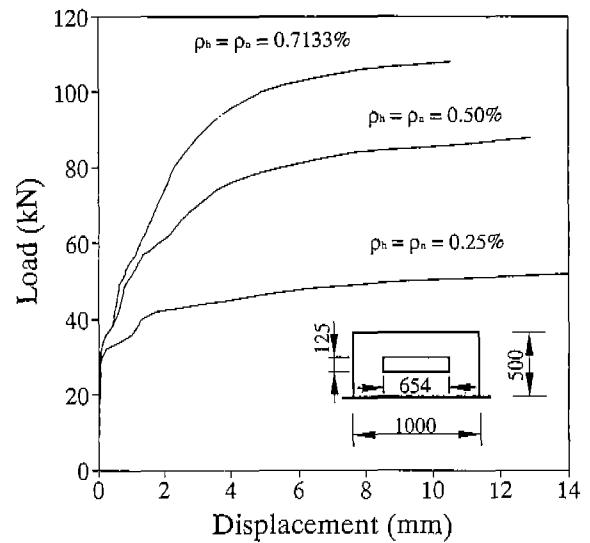


Fig. 5. Effects of Reinforcement Ratio.

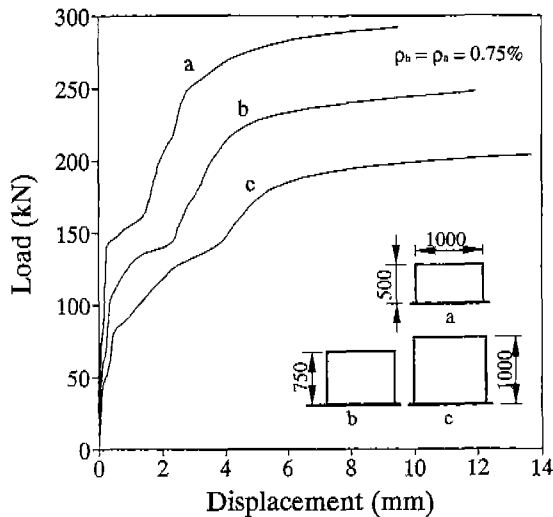


Fig. 4. Load-Displacement Curves with Change of Wall Height.

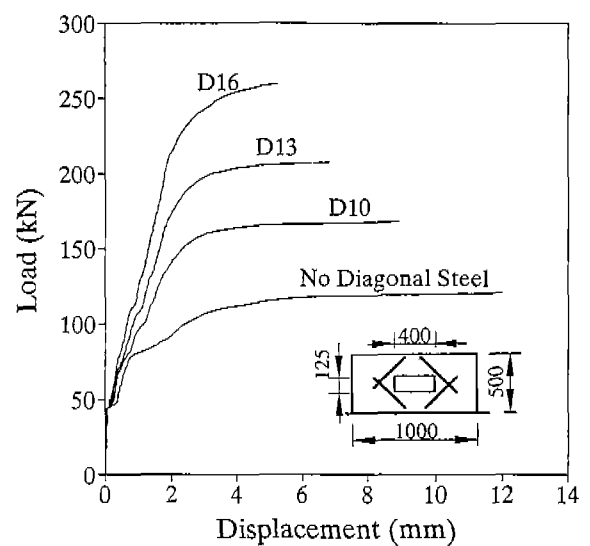


Fig. 6. Effects of Diagonal Reinforcement.

actually a particular case of a perforated shear wall with zero opening ratio.

Fig. 4 compares analytical results in terms of varying wall height. Length and thickness of the three walls are 1000 mm and 100 mm. Height differs at 500 mm, 750 mm and 1000 mm. Horizontal and vertical reinforcement ratios are 0.75%. Compressive strength of concrete is 25.4 MPa, and tensile strength of reinforcement is 510 MPa. The figure shows that load-displacement curves are similar in shape, and an increase in ultimate loading with a decrease in ductility is observed due to reduction of wall height.

A group of load-displacement curves for three perforated shear walls with changes in horizontal and vertical reinforcement ratios is shown in Fig. 5. Reinforcement ratios are 0.25%, 0.5% and 0.7133%. Opening size is 654

mm×125 mm. Compressive strength of concrete is 25.4 MPa, and tensile strength of reinforcement is 510 MPa. Before concrete cracks, the stiffness of these three cases is almost the same. Reinforcement thus plays a small role in resisting lateral force at the pre-cracking stage. After concrete cracks, the stiffness of shear walls is enhanced as reinforcement ratio increases. This suggests that an increase in both horizontal and vertical reinforcement effectively reduces propagation of cracks and carries the forces released by cracked concrete. Therefore, a reduction in horizontal and vertical reinforcement leads to an increase in ductility and a decrease in wall capacity.

Comparison of changing diagonal reinforcement for perforated shear walls is shown in Fig. 6. Overall dimensions

are 1000-mm long, 500-mm high and 100-mm thick with a 400 mm×125 mm opening; 0.5% of horizontal and vertical reinforcement ratios are selected for all cases. Diagonal reinforcement, 530-mm long, varies from none to 71.33 mm² (D10) to 126.7 mm² (D13) to 197.93 mm² (D16), and is placed at a 45° angle to the horizontal direction. Compressive strength of concrete is 25.4 MPa, and tensile strength of reinforcement is 510 MPa. The results show that at the pre-cracking stage, enlargement of diagonal reinforcement scarcely increases the walls stiffness. But at the post-cracking stage, stiffness of the shear wall is greatly increased with more diagonal reinforcement. This indicates that diagonal reinforcement has a significant effect on wall capacity. A reduction of diagonal reinforcement results in a decrease of stiffness after the appearance of cracks, and leads to a lessening of wall capacity.

All the shear wall behavior, as presented here, is derived from NFEM and conforms to experimental observations. Note that some theoretical results are self-evident, such as a reduction of wall capacity due to a decrease of reinforcement ratios. Overall, the behavior of shear walls is important in theoretical solutions since it is indispensable for examining the reliability of NFEM itself.

4. Load-displacement Relationships

Further investigation is conducted to develop load-displacement relationships for low-rise unbounded shear walls with or without openings. For solid shear walls, the effects of height, horizontal and vertical reinforcement ratio, compressive strength of concrete, and tensile strength of reinforcement are considered. These parameters for each wall are summarized in Table 3.

Experimental results (Barda *et al.*, 1977) show that, for low-rise shear walls with flanged boundary elements, vertical reinforcement plays a more important role in a walls

shear strength than horizontal reinforcement. ACI 318-95 building code (ACI, 1995) takes the effects of vertical reinforcement into account and provides the following equations.

$$\rho_n = 0.0025 + 0.5 \left(2.5 - \frac{h_w}{l_w} \right) (\rho_h - 0.0025) \tag{1}$$

$$0.0025 \leq \rho_n \leq \rho_h \tag{2}$$

where ρ_n , ρ_h =vertical and horizontal reinforcement ratio, respectively, h_w =height of shear wall, and l_w =length of shear wall.

Results of these equations to determine vertical reinforcement ratio by using horizontal reinforcement ratio as a basis are shown in Table 4. Note that, while height-to-length ratio changes from 0.5 to 1.0, there is little difference between horizontal and vertical reinforcement ratio. Thus the same ratio for horizontal and vertical reinforcement is adopted here for further investigation.

Table 5 presents dimensions of perforated shear walls, opening ratio, and material properties as well as horizontal, vertical, and diagonal reinforcement.

There are 16 cases of solid walls and 132 cases of perforated shear walls based on Table 3 and 5. For a 1000 mm×500 mm×100 mm solid shear wall with concrete compressive strength of 25.4 MPa and reinforcement tensile strength of 510 MPa, four cases are analyzed in which hor-

Table 3. Parameters of Solid Shear Walls

$l_w \times h_w \times h$ (mm)	$\rho_h = \rho_n$ (%)	f'_c (MPa)	f_y (MPa)	h_w/l_w
1000×500×100	0.25, 0.5, 0.75, 1.0	25.4	510	0.5
1000×750×100	0.25, 0.5, 0.75, 1.0	25.4, 29.4	510, 461.7	0.75
1000×1000×100	0.25, 0.5, 0.75, 1.0	25.4	510	1.0

Table 4. ρ_n , ρ_h with Change of Height-to-Length Ratio

	$h_w/l_w=0.5$				$h_w/l_w=0.75$				$h_w/l_w=1.0$			
ρ_h	0.0025	0.0050	0.0075	0.0100	0.0025	0.0050	0.00755	0.0100	0.0025	0.0050	0.0075	0.0100
ρ_n	0.0025	0.0050	0.0075	0.0100	0.0025	0.0047	0.0069	0.0091	0.0025	0.0044	0.0063	0.0081

Table 5. Parameters of Perforated Shear Walls

$l_w \times h_w \times h$ (mm)	Opening Ratio ρ_o	$\rho_h = \rho_n$ (%)	Diagonal Bars	f'_c (MPa)	$f_y = f_{yd}$ (MPa)	h_w/l_w
1000×500×100	0.1, 0.1635, 0.2	0.25, 0.5, 0.7133		25.4	510	0.5
1000×750×100	0.1, 0.15, 0.218	0.25, 0.5, 0.75, 1.0	None, D10(#3), D13(#4), D16(#5)	27.9	461.7	0.75
1000×1000×100	0.1, 0.15, 0.2	0.25, 0.5, 0.75, 1.0		27.9	461.7	1.0

horizontal and vertical reinforcement ratios change from 0.25%, 0.5%, 0.75% to 1.0%. For a 1000 mm×750 mm×100 mm solid shear wall, two material groups ($f'_c=25.4$ MPa, $f_y=510$ MPa, and $f'_c=29.4$ MPa, $f_y=461.7$ MPa) comprising eight cases are analyzed: horizontal and vertical reinforcement ratio change from 0.25% to 1.0%. For a 1000 mm×500 mm×100 mm perforated shear wall with 0.1 opening ratio (rate of opening area to product of wall height and length), and 0.25 horizontal and vertical reinforcement ratio, four cases are obtained with diagonal reinforcement varying from none to D16 (#5). Changes of dimension, opening ratio, horizontal and vertical reinforcement ratio, and diagonal reinforcement result in 132 cases for perforated shear walls. Based on NFEM solutions for the above cases and test results by Sheu (1988), cracking, yielding and ultimate load with corresponding displacements are obtained by regression and presented as follows.

Cracking load P_{cr} (N)

$$P_{cr} = [6.233 + 10.827\rho_o - 101.780\rho_o^2 + (6.398 + 9.834\rho_o) \left(\frac{l_w}{h_w}\right) + (1.542 - 24.618\rho_o) \left(\frac{l_w}{h_w}\right)^2] \times 10^{-3} l_w h f'_c \quad (3)$$

Cracking displacement Δ_{cr} (mm)

$$\Delta_{cr} = [1 + 4.4705\rho_o + 125.8122\rho_o^2 + (6.493 - 99.8875\rho_o + 174.0799\rho_o^2) \left(\frac{h_w}{l_w}\right) - (6.5325 - 98.0783\rho_o + 273.529\rho_o^2) \left(\frac{h_w}{l_w}\right)^2] \times \frac{\left(1 + \frac{3EIK}{A_c h_w^2 G}\right)}{3EI} h_w^3 P_{cr} \quad (4)$$

Yielding load P_y (N)

$$P_y = [1 - 44.366\rho_o - 249.074\rho_o^2 + (15.433 - 129.775\rho_o + 1103.385\rho_o^2) \left(\frac{l_w}{h_w}\right) + (1.650 - 26.705\rho_o + 461.869\rho_o^2) \left(\frac{l_w}{h_w}\right)^2] \times 10^{-3} l_w h f'_c + [0.272 - 8.151\rho_o + 34.180\rho_o^2 + (0.092 + 11.279\rho_o - 52.171\rho_o^2) \left(\frac{l_w}{h_w}\right) + (0.001 - 4.106\rho_o + 17.960\rho_o^2) \left(\frac{l_w}{h_w}\right)^2] \rho l_w h f_y + [0.758 - 0.667 \left(\frac{l_w}{h_w}\right) + 0.169 \left(\frac{l_w}{h_w}\right)^3] n A_d f_{yd} \cos \phi \quad (5)$$

Yielding displacement Δ_y (mm)

$$\Delta_y = \{0.0024 - 0.0408\rho_o + 0.2070\rho_o^2 + (0.7442 + 0.0085\rho_o - 21.5337\rho_o^2)\rho + [0.4639 - 6.0695\rho_o + 19.1698\rho_o^2 - (9.537 - 1.9278\rho_o - 339.1297\rho_o^2)\rho - (0.4590 - 6.8013\rho_o + 22.7969\rho_o^2) \left(\frac{h_w}{l_w} - 0.1\right)^{10\rho} \frac{f'_c}{f_y} + (6.2330 + 32.8707\rho_o - 120.6860\rho_o^2) \frac{f'_c}{f_y} \rho_d\} \sqrt{l_w h_w} \quad (6)$$

Ultimate load P_u (N)

$$P_u = [1 + 505.033\rho_o - 2118.820\rho_o^2 + (11.843 - 601.298\rho_o + 2564.563\rho_o^2) \left(\frac{l_w}{h_w}\right) + 45.341\rho_o^2 + (0.024 + 13.269\rho_o - 62.696\rho_o^2) \left(\frac{l_w}{h_w}\right) + (0.001 - 4.529\rho_o + 20.497\rho_o^2) \left(\frac{l_w}{h_w}\right)^2] \rho l_w h f_y + [0.024 \left(\frac{l_w}{h_w}\right) + 0.094 \left(\frac{l_w}{h_w}\right)^3] n A_d f_{yd} \cos \phi \quad (7)$$

Ultimate displacement Δ_u (mm)

$$\Delta_u = \{0.0178 - 0.0564\rho_o + 0.2050\rho_o^2 - (0.9243 + 0.0173\rho_o - 52.3631\rho_o^3)\rho + [0.3008 - 0.8848\rho_o - 24.1924\rho_o^2 + (4.6108 + 62.9711\rho_o - 1209.9000\rho_o^2)\rho - (0.2844 - 1.3419\rho_o - 25.9565\rho_o^2) \left(\frac{h_w}{l_w} - 0.1\right)^{10\rho} \frac{f'_c}{f_y} - (0.8176 - 4.9281\rho_o + 20.4290\rho_o^2) \frac{f'_c}{f_y} \cdot 4\sqrt{\rho_d}\} \sqrt{l_w h_w} \quad (8)$$

where $\rho_o = A_o/A_c$, opening ratio; A_o =opening area (mm²); A_c =area of shear wall $l_w \times h_w$ (mm²); h_w =height of shear wall (mm); l_w =length of shear wall (mm); f'_c =compressive strength of concrete (MPa); ρ =reinforcement ratio (smaller value is selected if difference between horizontal and vertical reinforcement ratio is slight); h =thickness of shear wall (mm); f_y =tensile strength of reinforcement (MPa); A_d =area of one piece of diagonal reinforcement (mm²); f_{yd} =tensile strength of diagonal reinforcement (MPa); $\phi=45^\circ$ angle between diagonal reinforcement and horizontal direction; $G = \frac{E}{2(1+\nu)}$, shear modulus of concrete (MPa); $\rho_d = \frac{n A_d}{l_w h_w} \cos \phi$, equivalent diagonal reinforcement ratio; n =number of diagonal reinforcement at cross section $l_w \times h$; E =initial modulus of concrete (MPa); ν =Poisson's ratio; I =moment of inertia (mm⁴); K =numerical factor (1.2). These notations are illustrated in Fig. 7. Note that

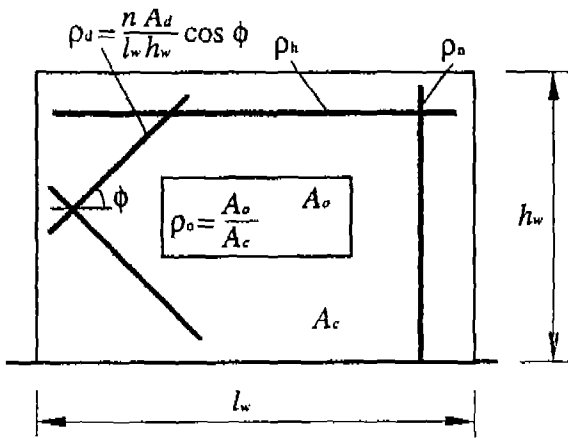


Fig. 7. Definition of Symbols for Shear Walls.

Table 6. Coefficient for Determination of R^2 in Eqs. (3) through (8)

Equation	(3)	(4)	(5)	(6)	(7)	(8)
R	0.9916	0.9988	0.9753	0.9108	0.9760	0.8278

Eqs. (3) through (8) can also be applied to solid shear walls assuming the opening ratio equals to zero.

Statistical measurement of the coefficient of determination (R^2) for Eq. (3) through (8) is shown in Table 6.

Though Eqs. (3) through (8) are derived from mathematical curve-fitting, the selection of variables for regression has a rational basis in shear wall behavior. These equations thus fully reflect the characteristics of shear wall at the cracking, yielding and ultimate stages.

Experimental and computational results indicate that the load-displacement relationship stays linear until concrete cracks. Low stresses in reinforcement mean that concrete mainly resists applied load at the pre-cracking stage. The role of reinforcement under cracking load can be neglected with satisfactory accuracy. Therefore, cracking load of Eq. (3) is proportional to the shear-wall cross-section and concrete compressive strength. An increase in opening ratio and wall height results in the reduction of cracking load.

For solid shear walls, lateral displacement at the cracking stage can be easily determined applying the principle of mechanics of material with consideration of shear deformation. A coefficient, which reflects the influence of opening ratio and the wal's height-to-length ratio, is introduced to revise the lateral displacement of a solid shear wall. Thus the application of cracking displacement in Eq. (4) is extended to perforated low-rise shear walls.

Equations (5) and (7) for yielding and ultimate load are based on the sum of contributions of concrete, horizontal and vertical reinforcement, and diagonal reinforcement. Each term is modified by the length-to-height ratio. Terms

of concrete as well as vertical and horizontal reinforcement are also considered in the effect of opening ratio, because the existence of an opening reduces the walls cross-section and the amount of vertical and horizontal reinforcement.

Both experimental and analytical results show that an increase in vertical, horizontal, and diagonal reinforcement will reduce shear wall ductility. An increase in opening ratio and wall height will increase ductility. These findings provide the basis of Eqs. (6) and (8).

From analytical and experimental results in Fig. 2, the slope of a load-displacement curve is not greatly reduced at the beginning of vertical reinforcement yielding. This is due to uniform distribution of vertical reinforcement and relatively sizeable length l_w of cross section. Thus yielding load is defined as the beginning of significant change in the slope of a load-displacement curve.

To establish the load-displacement curve, a straight line is used to depict the relationship between lateral load and displacement before concrete cracks. Stiffness of the curve at the pre-cracking stage is determined by P_{cr}/Δ_{cr} . Then pre-cracking load can be obtained by the stiffness times given displacement. The load-displacement relationship between the yielding and ultimate stage of a wall is also represented by a straight line. For the region between a wall's cracking and yielding load, the load-displacement relationship is described by a second-order polynomial.

$$P = \alpha \Delta^2 + \beta \Delta + \gamma \tag{9}$$

In Eq. (9), load P reaches cracking load P_{cr} with corresponding displacement Δ_{cr} , and the load becomes yielding load P_y when Δ equals yielding displacement Δ_y . The slope at Δ_y is assumed to be equal to that of a straight line for post-yielding load in order to achieve a smooth transition from a second-order polynomial to a straight line at the point of yielding load. Parameters α , β , and γ in Eq. (9) can be derived as

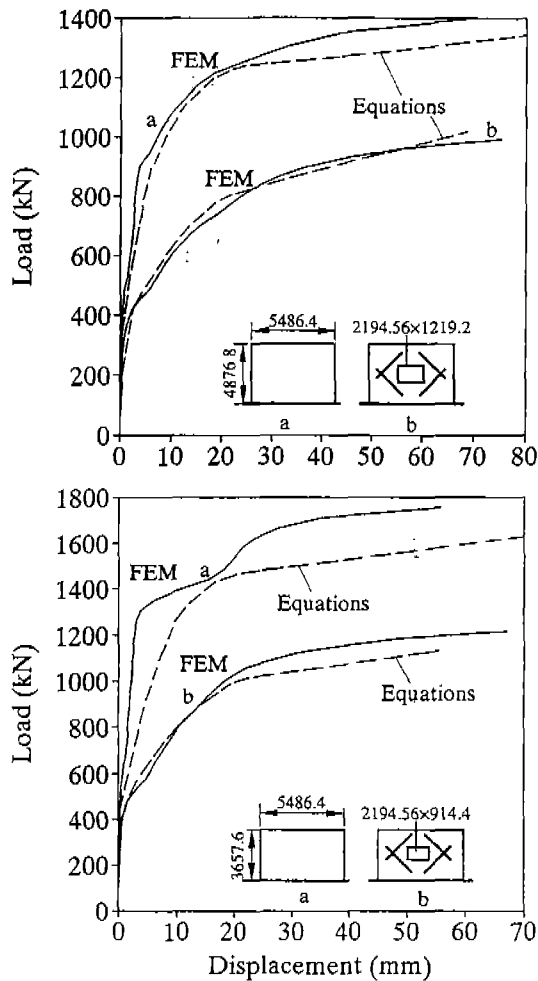
$$\alpha = \frac{\Delta_y - \Delta_{cr}(P_u - P_y) + P_{cr} - P_y}{(\Delta_y - \Delta_{cr})^2} \tag{10}$$

$$\beta = \frac{2\Delta_y(P_y - P_{cr}) \frac{\Delta_y^2 - \Delta_{cr}^2}{\Delta_u - \Delta_y} (P_u - P_y)}{(\Delta_y - \Delta_{cr})^2} \tag{11}$$

$$\gamma = P_{cr} - \frac{\Delta_{cr}}{(\Delta_y - \Delta_{cr})^2} [(P_y - P_{cr})(2\Delta_y - \Delta_{cr}) - \frac{\Delta_y - \Delta_{cr}}{\Delta_u - \Delta_y} (P_u - P_y)\Delta_y] \tag{12}$$

Table 7. Properties of Solid and Perforated Shear Walls

$l_w \times h_w \times h$ (mm)	Opening Area (mm ²)	ρ_o	f'_c (MPa)	$\rho_h = \rho_n$ (%)	A_d (mm ²)	$f_y = f_{yd}$ (MPa)	h_w/l_w
5486.4×3657.6×152.4	None	0	28.148	0.55	None	422.22	0.67
	2194.56×914.4	0.1			4×129		
5486.4×4876.8×152.4	None	0	28.148	0.55	None	422.22	0.89
	2194.56×1219.2	0.1			4×129		

**Fig. 8.** Prediction of Load-Displacement Curves for Shear Walls.

These proposed load-displacement equations of low-rise unbounded shear walls with or without openings demonstrate that: (1) shear walls with larger openings have lower capacity with greater ductility; (2) an increase in wall height leads to an increase in ductility and a reduction in capacity; and (3) a decrease in horizontal and vertical or diagonal reinforcement leads to an increase in ductility and a reduction in wall capacity. These characteristics hold true for low-rise shear walls with or without openings. Comparison of test results,

computer solutions and proposed equations (see Fig. 2) shows a good conformation.

Through the proposed equations, further comparisons are presented to predict the behavior of four large-scale low-rise shear walls with or without openings, selected from a three-story commercial building in Pleasant, California (Calif. Dept. of Conservation, 1989). Dimensions and material parameters of these walls are shown in Table 7. Fig. 8 compares results of NFEM and proposed equations. In general, they conform well with each other at cracking, yielding and ultimate stages. The largest deviation of proposed equations and NFEM results is observed from the solid shear wall 3657.6-mm high. Ultimate loading values from NFEM and the proposed equations are 1755 kN and 1596 kN, respectively. The latter is approximately 91% of the former. Such an error is acceptable.

5. Capacity of Low-rise Shear Walls

Low-rise unbounded RC shear walls, especially without openings, feature equal vertical and horizontal reinforcement ratios. Due to this state of equality, shear-wall failure modes, whether shear or flexure, are dominated by reinforcement ratios and wall height. However, Eq. (7) gives only shear-wall theoretical capacity, and does not indicate which failure mode occurs at the ultimate stage. A fuller understanding is needed for shear-wall failure behavior. Toward this end, further study is presented below based on a comparison of NFEM solutions and ACI 318-95 building code provisions (ACI 1995) for a wall's shear strength. This endeavor may help to judge the possible failure modes of a shear wall, and offer a method to evaluate shear wall capacity. Discussion of capacity here focuses on low-rise solid shear walls since no specific provisions for the design of perforated shear walls in ACI 318-95 are available for comparison.

Shear Strength Based on ACI Building Code

ACI 318-95 building code provides the following equations in Chapter 11 to calculate shear strength V (in metric units).

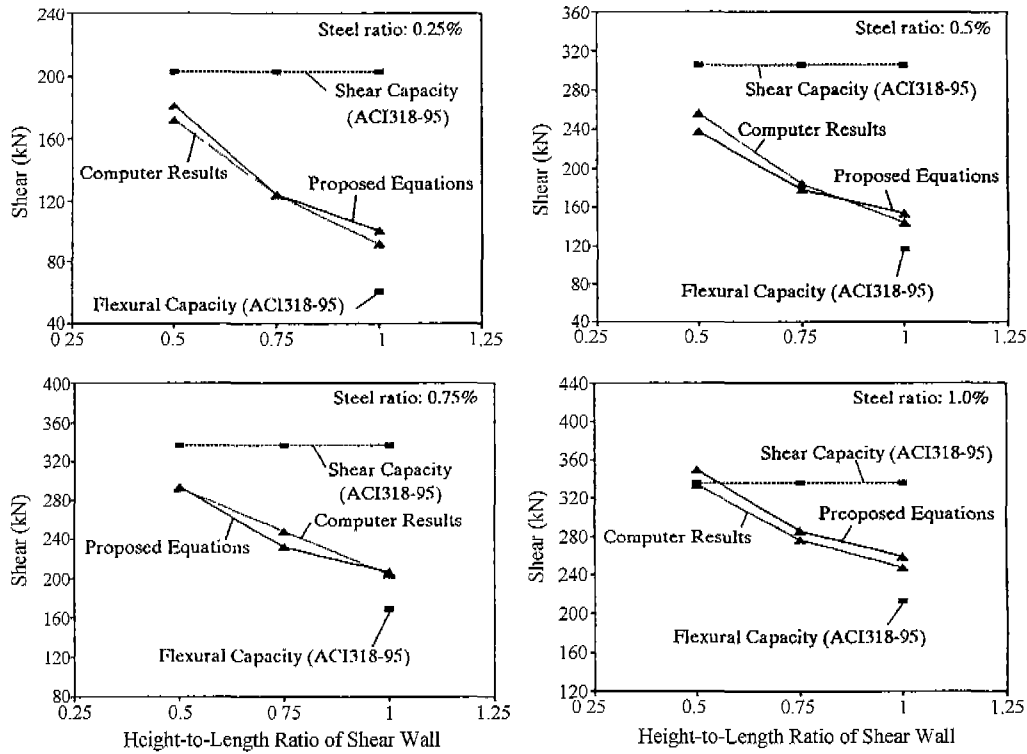


Fig. 9. Comparison of Shear Capacity.

$$V = \frac{1}{4}\sqrt{f_c}hd + \frac{A_v f_y d}{s} \tag{13}$$

$$\text{or } V = \frac{1}{10} \left[\frac{1}{2}\sqrt{f_c} + \frac{\sqrt{f_c} l_w}{\frac{M}{V} - \frac{l_w}{2}} \right] hd + \frac{A_v f_y d}{s} \tag{14}$$

$$V \leq \frac{5}{6}\sqrt{f_c}hd \tag{15}$$

where d =distance from extreme compression fiber to centroid of longitudinal tension reinforcement, or $0.8h$ (mm); s =spacing of horizontal shear reinforcement (mm); A_v =area of horizontal shear reinforcement within a distance s ; M =moment at the section above the height of l_w . Other notations are the same as Eqs. (3) through (8).

Shear strength comes from the least value in Eqs. (13), (14) and (15). For low-rise shear walls, $\frac{M}{V} - \frac{l_w}{2}$ is negative and Eq. (14) does not apply. Shear strength is determined by Eqs. (13) and (15). Vertical shear reinforcement is calculated from Eqs. (1) and (2).

Failure Modes of Solid Low-Rise Shear Walls

For low-rise unbounded solid shear walls (100-mm wide and 1000- mm long with height varying from 500 mm to 1000 mm), Fig. 9 summarizes comparisons of computer results, solutions from Eq. (7), and both shear and flexural strength of ACI building code. Compressive strength of con-

crete f'_c is 25.4 MPa, and tensile strength of reinforcement f_y is 510 MPa. Note that Eq. (7) can be simplified as follows since the opening ratio is zero for solid wall.

$$P_u = \left[1 + 11.843 \left(\frac{l_w}{h_w} \right) + 6.177 \left(\frac{l_w}{h_w} \right)^2 \right] \times 10^{-3} l_w h f'_c + \left[0.388 + 0.024 \left(\frac{l_w}{h_w} \right) + 0.001 \left(\frac{l_w}{h_w} \right)^2 \right] \rho l_w h f_y \tag{16}$$

In ACI code, the flexural strength of shear walls is mainly controlled by concrete and flexural reinforcement. The method of determining flexural strength is based on (1) static equilibrium, (2) linear distribution of concrete and reinforcement strains, and (3) material constitutive laws. However, this method cannot be applied to low-rise shear walls because lower wall's height-to-length ratio results in nonlinear strain and stress distribution. Since ACI 318-95 does not provide a specific method to evaluate low-rise shear-wall flexural strength, Fig. 9 presents only the flexural strength for shear wall's with a height-to-length ratio of 1.

Results in terms of ACI 318-95 indicate that shear strength based on Eqs. (13) through (15) is independent of wall height if the shear reinforcement ratio of low-rise shear walls is constant. If the height-to-length ratio decreases to 0.5, then the wall capacity in Eq. (16) is close to shear strength based on ACI code regardless of rein-

forcement ratio. This implies that shear walls will exhibit the shear failure mode. If height-to-length ratio increases to 1, then the wall capacity in Eq. (16) is much lower than shear strength obtained from ACI code. But wall capacity is close to flexural strength at a height-to-length ratio of 1, where flexural failure occurs. This conclusion gives a theoretical demonstration that an increase in wall height may change the failure mode from shear to flexure, a phenomenon already observed from tests.

Flexural Reinforcement in Low-Rise Bounded Shear Walls

Figure 9 indicates that if a low-rise shear wall is designed to have identical strength in shear and flexure, additional flexural reinforcement is required. This reinforcement is usually placed at both sides of the wall as an efficient way of giving the wall maximum resistance. This concept leads to an effective design method for low-rise bounded shear walls.

To determine flexural reinforcement, use Eqs. (13) to (15) to calculate horizontal shear reinforcement based on shear-wall design requirements. Then determine vertical shear reinforcement by using Eqs. (1) and (2). To make a wall's flexural strength and shear strength the same, the contribution of flexural and vertical shear reinforcement involves two parts of flexural strength. The first part, from by vertical shear reinforcement, is the ultimate load of Eq. (16) multiplied by wall height. The second part, from flexural reinforcement, is the difference between (a) required flexural strength and (b) flexural strength of the first part. If the difference is greater than zero, then flexural reinforcement can be computed using an internal lever arm equal to $0.6 h_w$, as proposed by Park and Paulay (1975) for deep beam; since ACI code does not provide a method to calculate flexural reinforcement for low-rise shear walls.

The above procedure of determining flexural reinforcement is illustrated by the following case. Take a solid wall 5486.4-mm long, 152.4-mm wide and 4876.8-mm high, part of a three-story commercial building in Pleasant, California (Calif. Dept. of Conservation 1989). Horizontal and vertical shear reinforcement ratios are both 0.55%. Compressive strength of concrete f'_c is 28.15 MPa, and tensile strength of reinforcement f_s is 422 MPa. Based on Eqs. (13) through (15), the wall's shear strength is 2440 kN. Lateral force from Eq. (16) equals 1395 kN. Thus the flexural strength is $(2440-1395) \times 4876.8 \times 10^{-3} = 5096$ kN-m in order for shear and flexural failure to occur in the wall simultaneously. Using the internal lever arm of $0.6 h_w$, flexural reinforcement is $5096 \times 10^6 / (0.6 \times 4876.8 \times 422) = 4127$ mm²; which is placed in the shear-wall boundary element. This method leads to a great reduction of flexural

reinforcement. Usually flexural strength due to uniformly distributed vertical shear reinforcement is not considered in design practice. Thus required flexural reinforcement in the boundary element is $2240 \times 10^3 \times 4876.8 / (0.6 \times 4876.8 \times 422) = 9637$ mm². A 42% ($4127/9637=0.42$) reduction of flexural reinforcement is achieved if the flexural strength of vertical shear reinforcement is taken into account.

Advantages of this method are clear from the viewpoint of designing low-rise bounded shear walls: (1) consideration of flexural strength provided by vertical shear reinforcement can decrease the use of flexural reinforcement; (2) reduction of flexural reinforcement does not lead to a decrease in wall flexural strength, and may prevent the occurrence of shear or brittle failure; and (3) less reinforcement congestion in walls is expected.

6. Conclusions

Systematic studies of low-rise unbounded RC shear walls with or without openings are presented based on nonlinear finite element analysis and test comparison. To verify the reliability of NFEM algorithm presented by the authors, experimental results selected for comparison include nine shear panels tested by Vecchio and Chan, as well four low-rise unbounded shear walls tested by Sheu. These shear panels, with or without openings, are subjected to pure shear, combined shear and biaxial compression, and combined shear and biaxial tension, while low-rise unbounded shear walls, solid or perforated, represent those normally used in shear-wall design. Computer solutions successfully predict the failure mechanism of shear panels and shear walls, and conform well to test results. Also studied is the influence of a shear wall's height-to-length ratio, opening ratio, and horizontal and vertical reinforcement ratio as well as diagonal reinforcement. Based on computer solutions and test data, equations to predict cracking, yielding, and ultimate load with corresponding lateral displacement are established by regression, and give load-displacement curves for low-rise unbounded solid or perforated shear walls. These empirical equations, having a rational basis of shear wall behavior, (1) reflect shear-wall characteristics observed from analysis and tests, (2) express the relationship between solid and perforated shear-wall capacity, (3) establish backbone curve for inelastic analysis of shear-wall structures, and (4) display a good approximation to numerical and test results. Using these equations, practitioners can conveniently evaluate load-displacement relationships for low-rise unbounded shear walls.

Also, failure modes of low-rise unbounded shear walls

are theoretically investigated in order to judge the shear-wall failure mechanism during structural analysis. Comparison of analytical results and corresponding ACI 318-95 building code provisions indicates that an increase in wall height changes the failure mode from shear to flexure, a phenomenon already reported from test results. Shear-flexural failure can be obtained by adding additional flexural reinforcement in order to increase a wall's capacity. This concept is further extended to designing low-rise bounded shear walls and results in a design method to reduce flexural reinforcement. Use of this method can lessen the congestion of reinforcement in low-rise bounded shear walls and avoid unexpected shear or brittle failure.

Acknowledgments

This research work is partially supported by the National Science Foundation under grant NSF CMS 9416463. The support is gratefully acknowledged. Test results are based on joint research projects between F. Y. Cheng at University of Missouri-Rolla and M. S. Sheu at National Cheng Kung University in Taiwan. The Authors also acknowledge the technical advice provided by Dr. J. F. Ger, Assistant Bridge Engineer, Federal Highway Administration, Tallahassee, Florida.

References

- ACI (1983) Building Code Requirements for Reinforced Concrete, ACI 318-83, Detroit, Mich.
- ACI (1995) Building Code Requirements for Reinforced Concrete and Commentary, ACI 318-95/318R-89, Detroit, Mich. Anderson FE, Hanson RJ, Murphy HL, Newmark NM, Merit
- PW (1964) Design of Structures to Resist Nuclear Weapons Effects, ASCE, New York, N. Y.
- Antebi J, Utku S, Hanson RJ (1960) The Response of Shear Walls to Dynamic Loads, Rep., Dept. of Civ. and Sanitary Engrg., MIT, Cambridge, Mass.
- Barda F, Hanson JM, Corley WG (1976) An investigation of the design and repair of low-rise shear walls, PCA Res. and Development Bull., RD035D, PCA, Skokie, Ill.
- Barda F, Hanson JM, Corley WG (1977) Shear strength of low-rise walls with boundary elements, Reinforced Concrete Structures in Seismic Zones, SP 53-8, ACI, Detroit, Mich: 149-202.
- Benjamin JR, Williams HA (1957) The behavior of one-story reinforced concrete shear walls, J. Struct. Engrg. Div., ASCE, 83(3): 1254-1-1254-49.
- Cardenas AE, Hanson JM, Corley WG, Hognestad E (1973) Design provisions for shear walls, ACI J. 70(23): 221-230.
- Cardenas AE, Russell HG, Corley WG (1980) Strength of low-rise structural walls, Reinforced Concrete Structures Subjected to Wind and Forces, SP 63-10, ACI, Detroit, Mich.: 221-241.
- Calif. Dept. of Conservation (1989) Strong-motion Records from the Santa Cruz Mountains (Loma Prieta), California, Earthquake of 17 October 1989, Div. of Mines and Geology, Office of Strong Motion Studies, Rep. OSMS: 89-06.
- Chen WF (1982) Plasticity in Reinforced Concrete, McGraw-Hill Inc.
- Cheng FY (2001) Matrix Analysis of Structural Dynamics: Applications and Earthquake Engineering, Marcel Dekker, Inc., New York, N.Y.
- Cheng FY, Lou KY (1995) Inelastic behavior and load displacement equations of low-rise RC solid and perforated shear walls, Urban Disaster Mitigation: the Role of Engineering and Technology, Elsevier Science Ltd., F. Y. Cheng and M. S. Sheu, eds.: 79-96.
- Cheng FY, Lou KY, Yang JS (1994) Analytical and experimental studies of RC structures with low-rise shear walls, Proc., 5th U. S. Natl. Conf. on Earthquake Engrg., Chicago, Ill., 1: 45-54.
- Cheng FY, Mertz GE, Sheu MS, Ger JF (1993) Computed versus observed inelastic seismic low-rise RC shear walls, J. Struct. Engrg., ASCE, 119(11): 3255-3275.
- Cheng FY, Mertz GE (1991) Macro-model for inelastic low-rise RC shear walls, Proc., 10th Conf. on Electronic Computation, ASCE: 155-164.
- Cheng FY (1989) Coupling bending and shear hysteretic model of low-rise RC walls, Earthquake Concrete in Shear, Elsevier Science Ltd., Thomas Hsu and S. T. Mau, eds.: 276-288.
- Galletly GD (1952) Behavior of reinforced concrete shear walls under static load, Rep., Dept. of Civ. and Sanitary Engrg., MIT, Cambridge, Mass.
- Lou KY, Cheng FY (1994) NARCS: A computer Program for Non-linear Analysis of Reinforced Concrete Structures, Dept. of Civ. Engrg., Univ. of Missouri-Rolla, Rolla, MO.
- Lou KY, Ger JF, Yang RJ, Cheng FY (2001) Post-earthquake assessment of Mission-Gothic undercrossing, Computational Structural Engineering: An International Journal 1(1): 1-9
- Murakami H, Itoh M, Nishikawa T, Yokono K, Irino K, Torita H (1989) Structural characteristics of shear walls unframed by columns and beams, Trans., 10th Int. Conf. on Struct. Mech. in Reactor Tech., Vol. H, AASMiRT: 251-256.
- Ottosen NS (1977) A failure criterion for concrete, J. Engrg. Mech. Div., ASCE, 103(4): 527-535.
- Ottosen NS (1979) Constitutive model for short-time loading of concrete, J. Engrg. Mech. Div., ASCE, 105(1): 127-141.
- Park R, Paulay T (1975) Reinforcement Concrete Structures, Wiley Inter-Science, New York.
- Sheu MS (1988) Behavior of Low-rise RC Shear Walls Subjected to Reversed Cyclic Loading, Tech. Rep. to National Science Council, Arch. Engrg. Dept., National Cheng Kung Univ., Tainan, Taiwan.
- Vecchio FJ, Chan CCL (1990) Reinforced concrete membrane elements with perforations, J. Struct. Engrg., ASCE, 116(9): 2344-2360.
- Wataba M, Fukuzawa R, Chiba O, Hatori T (1989) Study on load-deflection characteristics of heavily reinforced concrete shear walls, Trans., 10th Int. Conf. on Struct. Mech. in Reactor Tech., Vol. H,

AASMiRT: 209-214.

Yamada M, Kawamura H, Katagihara K (1974) Reinforced concrete shear walls with openings, *Shear in Reinforced Concrete*, SP 42-25, ACI, Detroit, Mich.: 559-578.

Yang JS, Cheng FY, Sheu MS (1992) Inelastic modeling and response of low-rise RC shear walls and systems, *Proc., 10th World Conf. on Earthquake Engrg.*, Madrid, Spain, 8: 4313-4319.

Wood SL (1990) Shear strength of low-rise reinforced concrete walls, *J. ACI Struct.*, 87(1):99-107

Appendix I. Notations

The following symbols are used in this paper:

A_c	= area of shear wall $l_w \times h_w$ (mm^2)	G	= shear modulus of concrete (MPa)
A_d	= area of one diagonal reinforcement (mm^2)	h	= thickness of shear wall (mm)
A_o	= area of opening (mm^2)	h_w	= length of shear wall (mm)
A_v	= area of shear reinforcement within a distance s	I	= moment of inertia (mm^4)
d	= distance from extreme compression fiber to centroid of longitudinal tension reinforcement (mm)	K	= numerical factor (1.2)
E'	= initial elastic modulus of concrete (MPa)	M	= moment at cross section above height of l_w
f_c'	= compressive strength of concrete (MPa)	n	= number of diagonal reinforcement
f_y	= tensile strength of reinforcement (MPa)	P, P_{cr}, P_y, P_u	= load, cracking, yielding and ultimate load, respectively (N)
f_{yd}	= tensile strength of diagonal reinforcement (MPa)	s	= spacing of shear reinforcement (mm)
		V	= shear capacity (N)
		α, β	= parameters in Eq. (9)
		$\Delta, \Delta_{cr}, \Delta_y, \Delta_u$	= displacement, cracking, yielding and ultimate displacement, respectively (mm)
		ϕ	= 45° angle between diagonal reinforcement and horizontal direction
		γ	= parameters in Eq. (9)
		ρ	= smaller horizontal or vertical reinforcement ratio
		ρ_d	= equivalent diagonal reinforcement ratio
		ρ_h, ρ_n	= horizontal and vertical reinforcement ratio, respectively
		ρ_o	= opening ratio
		ν	= initial Poisson's ratio